

Article

N-Heterocyclic Carbene-Gold(I) Complexes Targeting Actin Polymerization

Domenico Iacopetta ^{1,*}, Jessica Ceramella ^{1,†}, Camillo Rosano ², Annaluisa Mariconda ³, Michele Pellegrino ¹, Marco Sirignano ⁴, Carmela Saturnino ^{3,5}, Alessia Catalano ⁶, Stefano Aquaro ¹, Pasquale Longo ⁴ and Maria Stefania Sinicropi ¹

¹ Department of Pharmacy, Health and Nutritional Sciences, University of Calabria, Via Pietro Bucci, Arcavacata di Rende, 87036 Cosenza, Italy; jessicaceramella@gmail.com (J.C.); michele.pellegrino@unical.it (M.P.); stefano.aquaro@unical.it (S.A.); s.sinicropi@unical.it (M.S.S.)

² Proteomics and Mass Spectrometry Unit, IRCCS Policlinico San Martino, L.go Rosanna Benzi 10, 16132 Genova, Italy; camillo.rosano@gmail.com

³ Department of Science, University of Basilicata, Viale dell'Ateneo Lucano 10, 85100 Potenza, Italy; annaluisa.mariconda@unibas.it (A.M.); carmela.saturnino@unibas.it (C.S.)

⁴ Department of Chemistry and Biology, University of Salerno, Via Giovanni Paolo II, 132, 84084 Fisciano, Italy; msirignano@unisa.it (M.S.); plongo@unisa.it (P.L.)

⁵ Spinoff TNcKILLERS, Viale dell'Ateneo Lucano 10, 85100 Potenza, Italy

⁶ Department of Pharmacy-Drug Sciences, University of Bari "Aldo Moro", 70126 Bari, Italy; alessia.catalano@uniba.it

* Correspondence: domenico.iacopetta@unical.it; Tel.: +39-098-449-3200

† These authors contributed equally to this work.



Citation: Iacopetta, D.; Ceramella, J.; Rosano, C.; Mariconda, A.; Pellegrino, M.; Sirignano, M.; Saturnino, C.; Catalano, A.; Aquaro, S.; Longo, P.; et al. N-Heterocyclic Carbene-Gold(I) Complexes Targeting Actin Polymerization. *Appl. Sci.* **2021**, *11*, 5626. <https://doi.org/10.3390/app11125626>

Academic Editor: Greta Varchi

Received: 10 May 2021

Accepted: 15 June 2021

Published: 18 June 2021

Publisher's Note: MDPI stays neutral with regard to jurisdictional claims in published maps and institutional affiliations.



Copyright: © 2021 by the authors. Licensee MDPI, Basel, Switzerland. This article is an open access article distributed under the terms and conditions of the Creative Commons Attribution (CC BY) license (<https://creativecommons.org/licenses/by/4.0/>).

Abstract: Transition metal complexes are attracting attention because of their various chemical and biological properties. In particular, the NHC-gold complexes represent a productive field of research in medicinal chemistry, mostly as anticancer tools, displaying a broad range of targets. In addition to the already known biological targets, recently, an important activity in the organization of the cell cytoskeleton was discovered. In this paper, we demonstrated that two NHC-gold complexes (namely **AuL4** and **AuL7**) possessing good anticancer activity and multi-target properties, as stated in our previous studies, play a major role in regulating the actin polymerization, by the means of *in silico* and *in vitro* assays. Using immunofluorescence and direct enzymatic assays, we proved that both the complexes inhibited the actin polymerization reaction without promoting the depolymerization of actin filaments. Our outcomes may contribute toward deepening the knowledge of NHC-gold complexes, with the objective of producing more effective and safer drugs for treating cancer diseases.

Keywords: NHC-gold complexes; actin; anticancer

1. Introduction

Transition metal complexes are considered candidates in medicinal chemistry because of their potential as new, diagnostic, and therapeutic agents. These complexes are modular systems in which the metal centers are bound to different ligands, arranged in a well-defined three-dimensional structure that determines the unique characteristics of the complexes. Transition metal complexes possess different photophysical/photochemical features, and numerous biological applications have been described [1–3]. Amongst the plethora of transition metal complexes, gold-based complexes are attracting the attention of many researchers, because of their possible oxidation states (e.g., Au(I) and Au(III)), stability, easy ligand exchange reactions, effective cytotoxicity towards several *in vitro* models of cancer, and the lack of negative effects on normal cell viability [4,5]. Gold has historically been used to treat several diseases, albeit the first scientific evidences date back to the 1920s, pertaining to the compound $K[Au(CN)_2]$ (potassium dicyanoaurate, Figure 1), which was clinically tested for its anti-tuberculosis activity, and then dismissed

because of its toxicity [6]. Instead, the literature shows many *in vitro* and *in vivo* studies conducted on the anticancer activities of another important gold-based complex, i.e., auranofin [(tetra-*O*-acetyl- β -D-glucopyranosyl)-thio] (triethylphosphine)-gold(I) (Figure 1), a second generation drug, which targets, in particular, the mitochondrial enzyme thioredoxin reductase (TrxR) [7]. These studies paved the way to the design, synthesis, and biological evaluation of many gold-based agents, mostly for the treatment of cancers. In this scenario, the gold complexes with N-heterocyclic carbene (NHC) ligands represent a challenging thread because of their ability to potently inhibit TrxR and decrease cancer cell proliferation [8,9]. However, TrxR is not the only target of anticancer gold complexes reported on so far. Indeed, amongst the other important functions, DNA and related enzymatic machinery interference [10], mitochondrial damage (mostly for cationic gold(I) biscarbene complexes) [11,12], and the inhibition of protein tyrosine phosphatases (PTP) [13] should also be noted. More recently, evidence indicated that NHC-gold complexes play an important role in regulating the cytoskeleton dynamics [14–18], interfering with the tubulin and/or actin metabolism. In our previous studies, we individuated two lead molecules, i.e., **AuL4** and **AuL7** (Figure 1) [15,18], demonstrating that they are good anticancer compounds and possess different biological properties, including the ability to regulate the tubulin polymerization reaction in two different ways. Indeed, **AuL4** is able to stabilize the tubulin filaments, behaving as one of the most well-known drug, paclitaxel, whereas **AuL7** hampers the tubulin polymerization reaction, such as the vinblastine, one of the most used vinca alkaloids that induces the assembly of tubulin into non-microtubule polymers, such as para-crystals or spiral proto-filamentous structures [19]. In this paper, another important biological target of the above-mentioned NHC-gold complexes has been studied, namely the actin, using as references the molecules latrunculin A (LA) and cytochalasin B (CB) (Figure 2). By using *in silico* and *in vitro* assays, we proved that both leads are able to inhibit the actin polymerization, with an efficacy similar to that of cytochalasin B (Phomin), a well-established cell-permeable fungal inhibitor of the actin polymerization. This evidence highlights, once again, the multi-target potential of the studied compounds, and is seminal for the development of potent and selective anticancer drugs targeting the actin, with negligible cytotoxic effects on the normal cells.

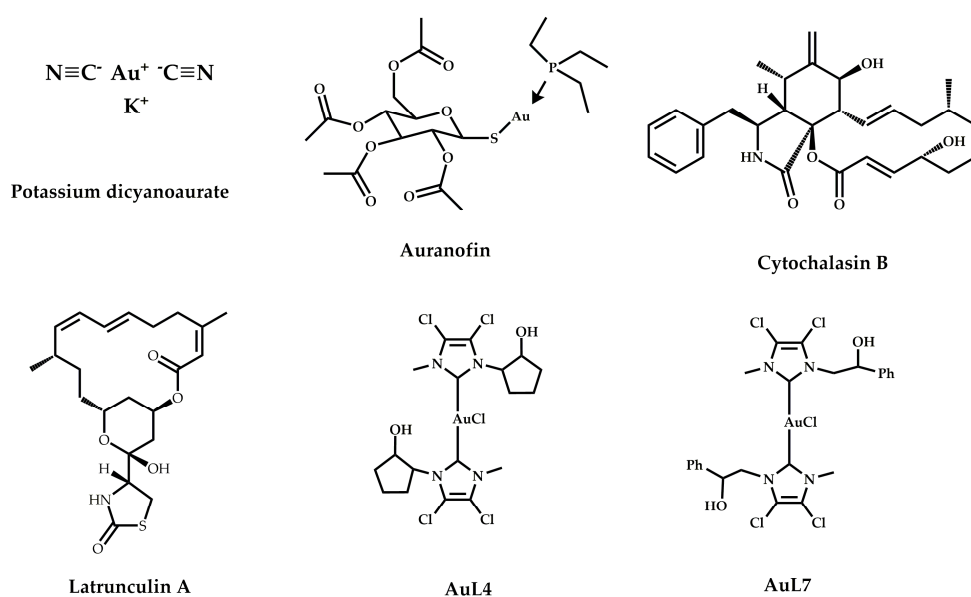


Figure 1. Molecular structure of potassium dicyanoaurate, auranofin, cytochalasin B, latrunculin A, **AuL4** and **AuL7**.

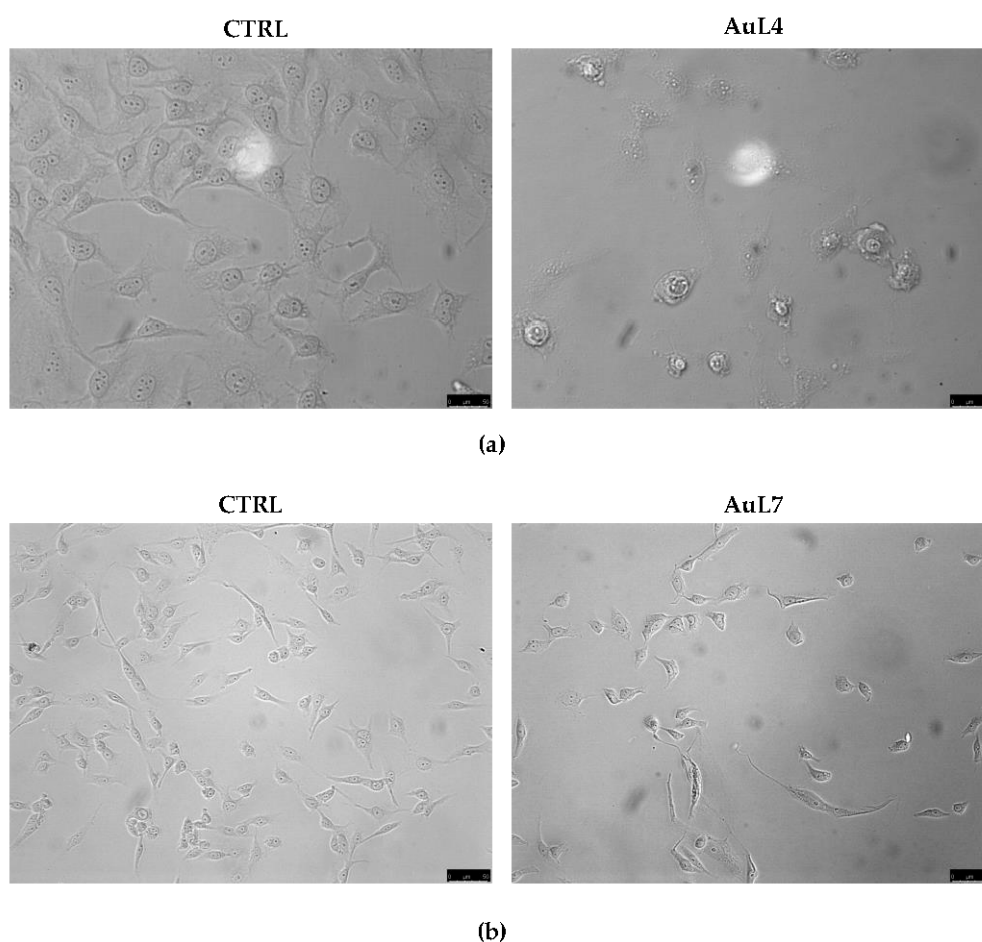


Figure 2. Morphological changes after the exposure of HeLa cells to **AuL4** (a) and MDA-MB-231 cells to **AuL7** (b). Both compounds were used at their IC_{50} values for 72 h. Images were acquired at $20\times$ magnification.

2. Materials and Methods

2.1. Cell Culture

The cell lines used in this work (MDA-MB-231 and HeLa) were purchased from American Type Culture Collection (ATCC, Manassas, VA, USA). Human breast cancer triple negative MDA-MB-231 were grown in DMEM-F12 medium containing 2 mmol/L L-glutamine, 1 mg/mL penicillin-streptomycin, and 5% Fetal Bovine Serum (FBS) [20]. HeLa human epithelial cervix carcinoma cells, estrogen receptor (ER)-negative were maintained in Eagle's minimum essential medium (MEM), supplemented with 10% FBS, 1% l-glutamine, 100 U/mL penicillin/streptomycin, and 1% non-essential amino acids (NEAA). All cell lines were maintained at 37 °C in a humidified atmosphere of 95% air and 5% CO_2 , and periodically screened for contamination [21].

2.2. Docking Studies

The crystal structure of the complex formed between the beta/gamma-actin with profilin and the acetyltransferase AnCoA-NAA80 [22] [PDB code 6nbw] was used as the protein target for our docking simulations. All structures of the ligands tested in silico were built, and energy was minimized using the program MarvinSketch (ChemAxon Ltd, Budapest, Hu). To shed light on the possible binding modes to the protein target and to determine their binding energies, we used the AutoDock v.4.2.2 program suite [23]. We performed a "blind docking" simulation: the docking of the small molecule to the targets was done without a priori knowledge of the location of the binding site by the system. All simulations were performed by adopting the program default values. The protein and the ligands were prepared using the ADT graphical interface [24]. Polar hydrogens were

added to each protein, Kollman charges assigned, and finally, the solvation parameters were added. The protein was considered a rigid object and all the ligands as fully flexible. A searching grid was extended all over the protein and affinity maps calculated. The search was carried out with a Lamarckian genetic algorithm: a population of 100 individuals with a mutation rate of 0.02 evolved for 100 generations. Evaluation of the results was performed by listing the different ligand poses according to their predicted binding energy. A cluster analysis based on root-mean-square-deviation (RMSD) values from the starting geometry was performed. The lowest energetic conformation of the most populated cluster was considered the best candidate. When clusters were almost equipopulated, and their energy distribution spread, their corresponding molecules were considered as bad ligands [25,26].

The generated docking poses were ranked in order of increasing binding energy values and clustered on the basis of a RMSD cut-off value of 2.0 Å. From the structural analysis of the lowest energy solutions of each cluster, we could spot the protein binding site. Figure 3 was drawn using the program Chimera [27].

2.3. Immunofluorescence Analysis

Cells were seeded in 48-well culture plates containing glass slides, serum-deprived for 24 h, and incubated with the most active compound for 24 h (concentration equal to its IC_{50} value). Then, the cells fixed with cold methanol were incubated with primary antibody, diluted in bovine serum albumin (BSA) 2% overnight at 4 °C, as previously described [28]. The rabbit anti- β -actin was purchased from Santa Cruz Biotechnology and diluted 1:100 before use. Then the secondary antibody Alexa Fluor[®] 488 conjugate goat-anti-rabbit (1:500, Thermo Fisher Scientific, MA, USA) was added and incubated for 2 h at 37 °C. Nuclei were stained using DAPI (Sigma Aldrich, Mila, Italy) for 10 min at a concentration of 0.2 μ g/mL. Fluorescence was detected using a fluorescence microscope (Leica DM 6000). LAS-X software was used to acquire and process all images.

2.4. Actin Polymerization/Depolymerization Assay

The ability of the tested compounds to interfere with the actin polymerization and depolymerization reaction was measured using an actin Polymerization/Depolymerization Assay Kit purchased from Abcam, following the manufacturer's instructions. Both polymerization and depolymerization reactions occur in a 100 μ L final volume, by using Labeled Rabbit Muscle actin reconstituted with the buffer G supplemented with 0.2 mM ATP and 0.5 mM DTT (1,4-dithiothreitol). For the polymerization assay, reconstituted actin was mixed with supplemented buffer G, and samples in a white 96-well plate, and then the polymerization, the reaction, was induced with the addition of the buffer P supplemented with 10 mM ATP. The solution was mixed and the data acquisition started. For the actin depolymerization assay, supplemented buffers P and G were mixed and incubated in a white 96-well plate at room temperature for one hour to polymerize the actin, protected from light. Then samples were added and the data acquisition started. Latrunculin A and cytochalasin B were used as control molecules at a concentration of 5 μ M. For both assays, the assembly of actin filaments was determined by measuring the fluorescence (Ex/Em: 365/410 nm) in kinetic mode for 1 h at room temperature using a microplate reader. Images are representative of three independent experiments, each performed in triplicate.

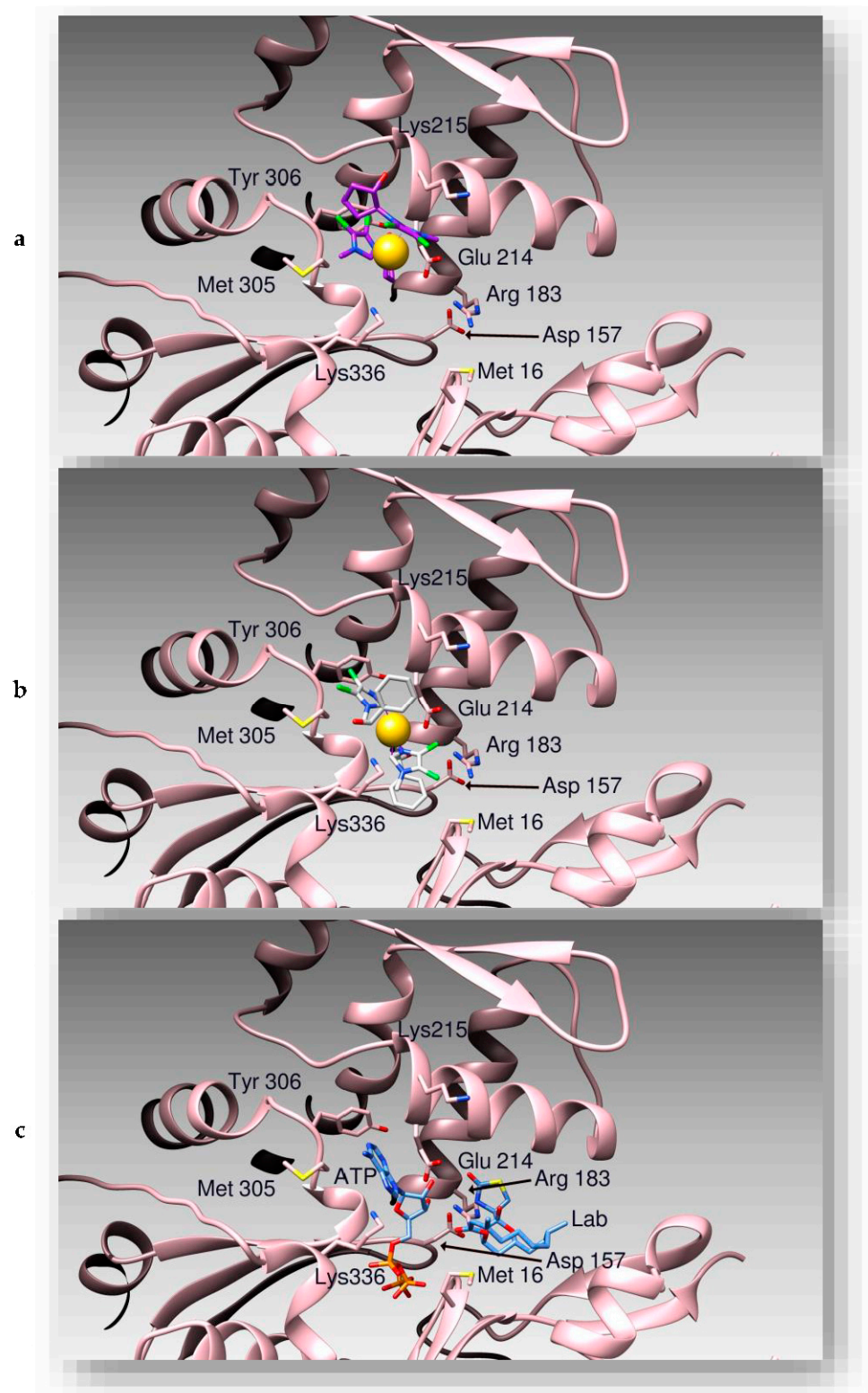


Figure 3. The three-dimensional structure of the nucleotide-binding cleft of actin (pink ribbon) is depicted. (a) **AuL4** pose; (b) **AuL7** pose; (c) binding mode of latrunculin B as determined by X-ray crystallography.

3. Results

3.1. **AuL4** and **AuL7** Induce Dramatic Cancer Cells Morphology Changes

Our previous studies demonstrated the anticancer activities of **AuL4** and **AuL7** against different in vitro models, being particularly effective against HeLa and MDA-MB-231

cancer cells, respectively, and triggering the ROS-mediated intrinsic apoptotic pathway. Moreover, we proved that these complexes possessed a multi-target action, namely they inhibited human topoisomerases I and II activities and interfered with the microtubules dynamics. However, this latter feature resides in the ability of **AuL7** to inhibit the tubulin polymerization reaction, acting like the vinblastine, whereas **AuL4** behaves as the paclitaxel, thus stabilizing the microtubules, as demonstrated by immunofluorescence and direct enzymatic assays. In both cases, the exposure of HeLa and MDA-MB-231 cancer cells to **AuL4** (at its $IC_{50} = 1.63 \pm 0.5 \mu M$) and **AuL7** (at its $IC_{50} = 2.1 \pm 0.7 \mu M$), respectively, for 72 h, produced dramatic morphological changes, as visible by the observation of cancer cells (Figure 2), using an inverted microscope (20 \times magnification). Indeed, **AuL4**-treated HeLa cells appeared round and shrunk, and **AuL7**-treated MDA-MB-231 cells exhibited both round and tread-like shapes, with respect to the vehicle-treated cells that have a normal morphology. These changes were attributed to the already proved interference with tubulin, but we wondered if our complexes could regulate the actin system, as well. This hypothesis sounded very challenging for us, because this would mean that the complexes possess another unexplored intracellular target, *viz.* the actin. In order to assess this supposition, we performed *in silico* and *in vitro* studies.

3.2. Docking Studies

To first evaluate the binding poses and the calculated affinities between **AuL4** and **AuL7** to the protein actin, we performed molecular docking simulations, using as a target the three-dimensional structure of actin [22]. Affinities of the two compounds to the protein were calculated by AutoDock, according to the expression $K_i = \exp(\Delta G / (R \cdot T))$. As discussed in our previous works [29–31], clusterization of the outcomes from our simulation runs, together with the visual inspection of the ligand:protein binding sites, were considered as markers of the quality of the interaction.

AuL4 and **AuL7** share the same actin binding site with latrunculin B (Figure 3), previously determined by X-ray crystallography [22]. Among the two compounds, **AuL4** is positioned within the nucleotide binding site of actin, forming hydrogen bonds with protein residues Asp211, Lys215, and Tyr306. Its chloride atoms are involved into halogen bonds with Glu214, while the gold atom is coordinated by Lys336. The binding site is stabilized by hydrophobic interactions with residues Met16, Met305, and Tyr306. On the other hand, **AuL7** is positioned with part of its structure exposed to the solvent. This compound forms hydrogen bonds with actin residues Asp157, Thr303, and the peptidic nitrogen atom of Gly182. Arg201 form a halogen bond with a chlorine atom of the ligand, which is also stabilized by hydrophobic interactions with Met16, Met305, and Tyr306. The Au atom is coordinated to Glu214.

3.3. **AuL4** and **AuL7** Interfere with the Normal Intracellular Actin Organization

The cell cytoskeleton is an important intracellular structure that is involved in several physiological processes, and is implied, as well, in tumor progression, most importantly in the epithelial–mesenchymal transition (EMT) process. The major components are tubulin and actin, which are targets of effective anticancer drugs. Some metal complexes have been proved to interfere with the cytoskeleton dynamics [15,32–36], particularly inhibiting the tubulin polymerization but, more recently, they were discovered to play a different and specific role in regulating the actin system [37]. Since we have already proved that the two metal complexes exerted inhibitory activity against the tubulin polymerization [15], we wondered whether they could also interfere directly with the other major component of the cell cytoskeleton, *viz.* the actin, in the two cancer cell models used for the previous study. With this in mind, HeLa and MDA-MB-231 cells were treated for 24 h with compounds **AuL4** (at its $IC_{50} = 1.63 \pm 0.5 \mu M$) and **AuL7** (at its $IC_{50} = 2.1 \pm 0.7 \mu M$), respectively, together with the only vehicle (DMSO, negative control). As a reference molecule, we used latrunculin A (positive control), a well-known natural compound that targets the actin cytoskeleton, at a concentration of 1 μM , under the same experimental conditions.

After that, cancer cells were further processed and imaged under a fluorescent microscope, as described in the Material and Methods section. As visible in Figures 4 and 5, in the negative control (only DMSO), the actin filaments exhibited a normal organization in the cell cytoplasm, with differences relative to the normal HeLa and MDA-MB-231 cell morphology. Conversely, under LA exposure, both cancer cell lines showed a remarkable disorganization of the actin system. Indeed, in Figure 4, the actin bundles are very thick and bright, with respect to the vehicle-treated HeLa cells, and one can notice that the actin system is more compact, not fairly distributed, and some dot-like structures appeared (see white arrows). A similar arrangement was seen in AuL4-treated HeLa cells; indeed, the cell size is reduced and the actin is thickened around the cell nuclei, with respect to the vehicle-treated cells (negative control). The MDA-MB-231 cells under AuL7 treatment lost their normal morphology, as well, but assumed different shapes; indeed, in Figure 5, some cells appear round, others with a thread-like structure or abnormally enlarged cytoplasm (see white arrows). Moreover, the actin filaments look very bright and arranged in dot-like structures or unevenly distributed within the cell cytoplasm. To summarize, we can affirm that both compounds interfere with the regular organization of the actin system in the cancer cells under investigation.

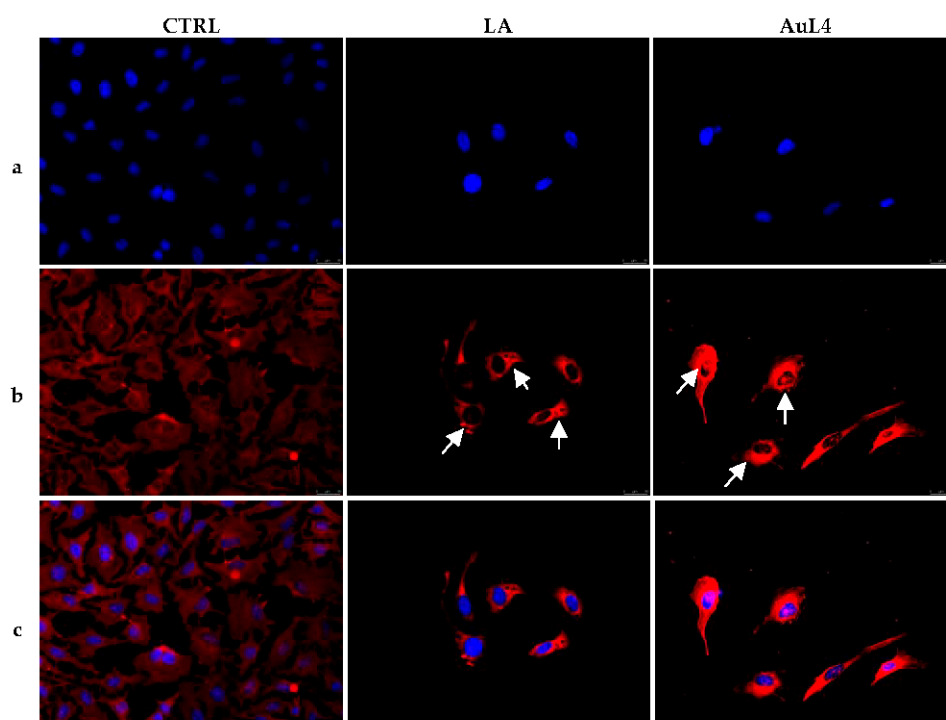


Figure 4. Immunofluorescence analysis. HeLa cells were treated with DMSO (CTRL, negative control) 0.1 μ M Latrunculin A (LA, positive control) or AuL4 (at its IC_{50} value) for 24 h. After treatment, the cells were further processed (see Materials and Methods section) and imaged under inverted fluorescence microscope at 20 \times magnification. In the CTRL cells, the actin filaments exhibited a normal organization in the cells cytoplasm. HeLa cells treated with LA and AuL4, showed an irregular arrangement and organization of the actin cytoskeleton: the actin system appear more compact, not fairly distributed and some dot-like structures appeared (see white arrows). (**Panels a**): nuclear stain with DAPI ($\lambda_{ex}/\lambda_{em}$ = 350/460 nm); (**Panels b**): β -actin (Alexa Fluor[®] 568; $\lambda_{ex}/\lambda_{em}$ = 644/665 nm); (**Panels c**): show the merge. Representative fields are shown.

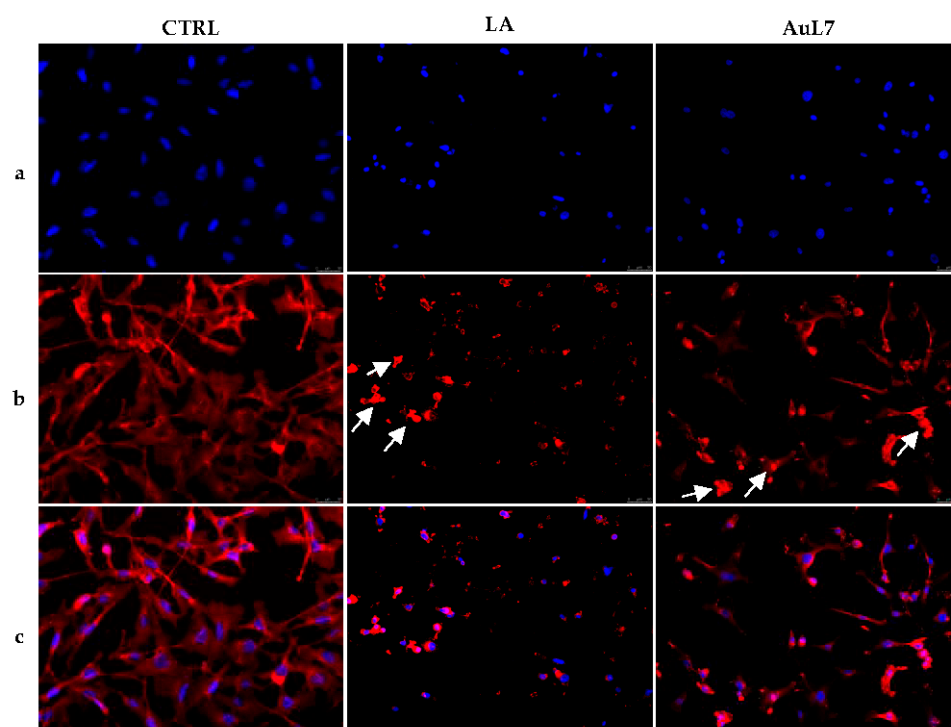


Figure 5. Immunofluorescence analysis. MDA-MB-231 cells were treated with DMSO (CTRL, negative control) 0.1 μ M Latrunculin A (LA, positive control) or **AuL7** (at its IC_{50} value) for 24 h. After treatment, the cells were further processed (see Materials and Methods section) and imaged under the inverted fluorescence microscope at 20 \times magnification (see Materials and Methods section). In the CTRL cells, the actin filaments exhibited a normal organization in the cells cytoplasm. Actin filaments in MDA-MB-231 cells treated with LA and **AuL7**, look very bright and arranged in dot-like structures: cells appear round and others with a thread-like structure (see white arrows). (**Panels a**): nuclear stain with DAPI ($\lambda_{ex}/\lambda_{em}$ = 350/460 nm); (**Panels b**): β -actin (Alexa Fluor[®] 568; $\lambda_{ex}/\lambda_{em}$ = 644/665 nm); (**Panels c**): show the merge. Representative fields are shown.

3.4. **AuL4** and **AuL7** Block the *In Vitro* Actin Polymerization Reaction but Do Not Accelerate the Depolymerization Reaction

Once established that the two metal complexes provoked a dramatic change of the cytoskeleton actin structure, we wondered whether the observed effect was due to a direct action toward the actin or through indirect effects, given that these compounds have already been proved as tubulin polymerization inhibitors. Thus, we adopted an *in vitro* actin assay that exploits a fluorescent-labeled purified rabbit actin, which polymerization/depolymerization reactions can be easily followed using a fluorimeter, in order to confirm the immunofluorescence results, and establish if **AuL4** and **AuL7** could act as actin polymerization inhibitors and/or accelerate the filamentous actin depolymerization. In this assay, we employed two reference molecules, namely the LA and CB. Particularly, LA can bind and sequester G-actin monomers, hampering the actin polymerization and, at the same time, accelerate the rate of the actin subunits dissociation from the assembled filaments. As a result, LA is able to block the F-actin formation, one way or another. Conversely, CB inhibits the actin polymerization, avoiding the monomers addition to the “barbed” end of the actin filaments, but it cannot increase the depolymerization reaction. The results from this assay were plotted and, as visible in Figure 6, in the control reaction (DMSO), the G-actin polymerizes very fast; indeed, the reaction curve reached a value of about 37,000 RFU (see experimental section for details), and kept the plateau until the end of the experiment. Conversely, the two reference molecules, LA and CB, used at a concentration of 5 μ M, blocked the actin polymerization; indeed, the initial rapid curve growth, seen in the control reaction, was absent. In more detail, the LA curve decreased until a value of about 12,000 RFU after 13–15 min and reached a value of about 10,000 RFU

at the end of the experiment. The exposure of actin monomers to CB produced a curve with a little increase (about 22,000 RFU) in the first 4–5 min, then decreased, and ended at an RFU value of 22,000, which is equal to the initial value. Finally, **AuL4** and **AuL7**, at a concentration equal to 5 μM , exhibited both an inhibiting activity similar to that of CB, and to a lesser extent, with respect to LA. Specifically, the **AuL4** curve was lower than that of CB in the first 5 min and then rose, maintaining RFU values ranging from 24,000 to 26,000, and ended at a final value of about 27,000 RFU. The **AuL7** curve trend was similar to that of **AuL4**, with the exception of the first 5 min, when it decreased to values lesser than LA, ending with a final value of 24,000 RFU. Overall, the inhibitory activity of **AuL7** seems better than **AuL4** but, in both cases, this assay demonstrates a direct effect on actin polymerization reaction, supporting the immunofluorescence assays.

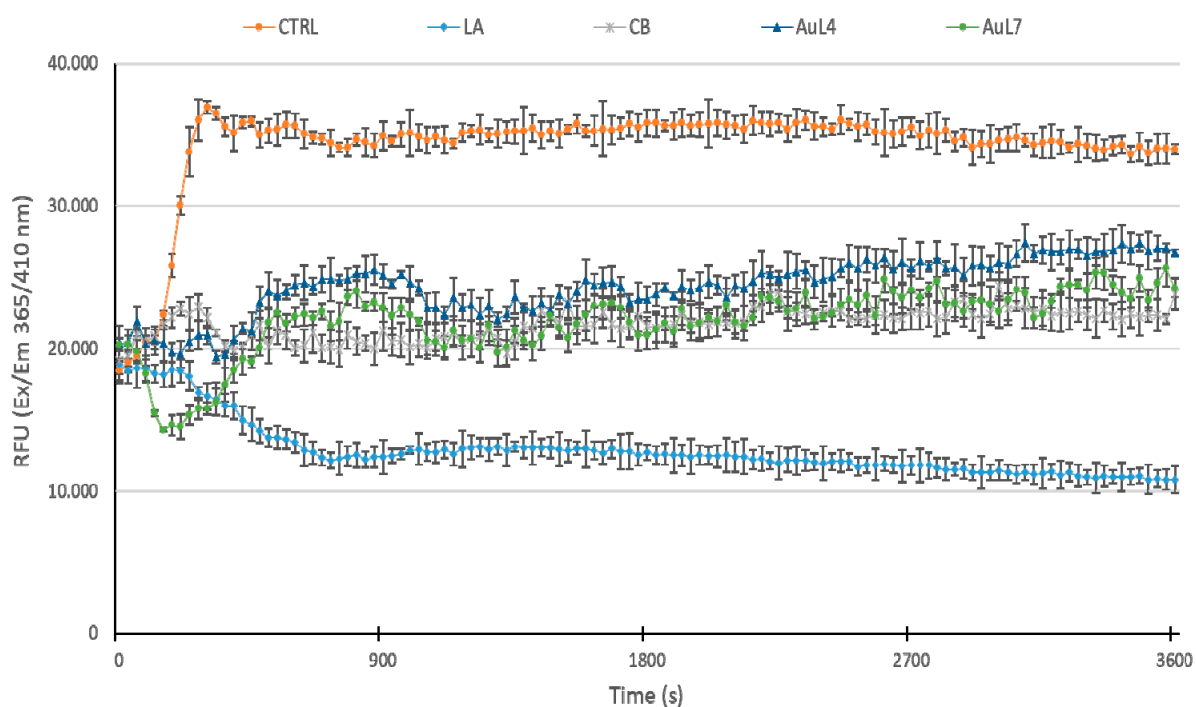


Figure 6. In vitro actin polymerization assay. The effect of compounds **AuL4** and **AuL7** (5 μM) on in vitro actin polymerization was examined. DMSO was used as a negative control (CTRL). Latrunculin A (LA) and cytochalasin B (CB), were employed as reference molecules and used at the concentration of 5 μM . **AuL4** and **AuL7**, incubated with the labeled rabbit muscle actin, demonstrate a direct effect on actin polymerization reaction. The graphic was obtained measuring the fluorescence (Ex/Em: 365/410 nm) given by actin filaments assembly in a kinetic mode for 1 h at room temperature. Data are representative of three independent experiments; standard deviations (SDs) are shown.

Considering that LA can trigger the F-actin disassembly, we performed a depolymerization assay, in order to determine whether our compounds could act as actin depolymerizing agents. Actin polymerization was allowed for one hour, under the same experimental conditions used in the previous assay, then **AuL4** or **AuL7** were added, at the concentration of 5 μM , and the reactions were monitored for one more hour. Negative (only vehicle and CB, 5 μM) and positive (LA, 5 μM) control reactions were performed, as well. Our results showed that the LA curve sensibly decreased until a value of 16,800 RFU in the first 8–9 min, meaning that the actin depolymerization was occurring (Figure 7). The initial value was around 28,000 RFU and after 9 min, the curve decreased slowly until the final value of 14,000 RFU. The negative control reactions (only vehicle and CB, 5 μM) showed no relevant changes, maintaining the same initial value and indicating that the F-actin did not depolymerize. The curves relative to **AuL4** and **AuL7** showed significant reduction in RFU values with respect to the control reactions, suggesting that they did not accelerate the depolymerization reaction. To summarize, these data proved that both **AuL4**

and **AuL7** are actin polymerization inhibitors with an efficacy similar to CB, used at the same concentrations and under the adopted experimental conditions, and do not accelerate actin depolymerization, contrarily to LA.

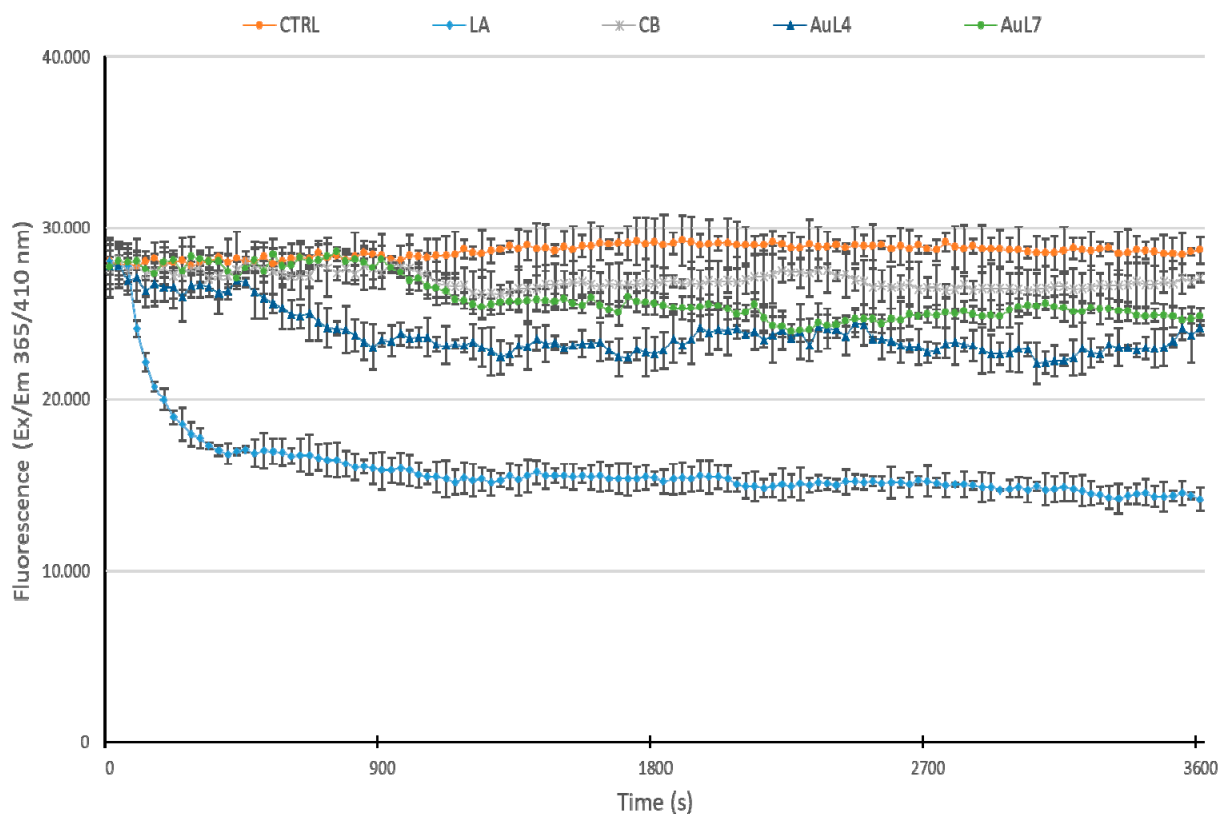


Figure 7. In vitro actin depolymerization assay. The effect of compounds **AuL4** and **AuL7** (5 μM) on in vitro actin depolymerization was examined. DMSO was used as a negative control (CTRL). Latrunculin A (LA) and cytochalasin B (CB), were employed as reference molecules and used at the concentration of 5 μM . **AuL4** and **AuL7**, added to the polymerized actin, do not accelerate the depolymerization reaction. The graphic was obtained measuring the fluorescence (Ex/Em: 365/410 nm) given by actin filaments disassembly in a kinetic mode for 1 h at room temperature. Data are representative of three independent experiments; standard deviations (SDs) are shown.

4. Discussion

Microtubules and actin filaments are cytoskeletal components that play pivotal roles in cell signaling, division, and motility, and regulate tumor relevant processes, for instance, morphological changes or cell migration [38]. For these reasons, they are interesting targets of an even higher number of anticancer drugs, such as the clinically used vinca alkaloids or taxanes that target microtubules, whereas compounds directed toward the actin have relatively lesser therapeutic applications, probably because of poor knowledge on their underlying mechanisms of action [39]. Under physiological conditions, the monomeric form of actin, called G-actin, polymerizes in a head-to-tail manner and constitutes the filamentous F-actin. The turnover of these forms is ensured by a tightly regulated equilibrium between G- and F-actin, but is substantially modified in cancer cells, together with changes in the filament-associated regulatory proteins, and is involved in the uncontrolled growth of tumor cells and, ultimately, in the increased ability to metastasize [40,41]. Generally, the migrating cancer cells undergo to shape rearrangements that depend on the formation of actin-based protrusions, cellular contractility, and new adhesions to surfaces [42]. For example, actin participates in the formation of specialized invasive and adhesive structures with proteolytic activity, called invadosomes [41]. Since we have already proved that the two NHC-gold complexes exerted inhibitory activity against the tubulin polymerization, we wondered whether they could also interfere directly with the other major component of the

cell cytoskeleton, *viz.* the actin. Indeed, some literature data reported that the actin system disorganization can be a consequence of the inhibition of the tubulin polymerization and not a direct regulation of the actin system [39,43]. Amongst the most well-known molecules able to interfere directly with the intracellular actin, different types of cytochalasin and latrunculin were employed in many research studies, because of their easy membrane permeation and different types of behavior against the actin polymerization and depolymerization processes. In our assays, we used, as reference molecules, cytochalasin B (CB), which inhibits the addition of monomers to the “barbed” end of the actin filaments [44], and latrunculin A (LA), which blocks the actin polymerization, and increases its depolymerization by trapping the actin monomers [45]. In our previous studies, we studied the anticancer properties of **AuL4** and **AuL7**, individuating some intracellular targets, as the human topoisomerases I and II, and the cytoskeleton tubulin, which decreased cancer cell growth by inducing the ROS-depending intrinsic apoptotic pathway. Encouraged by the outcomes, we continued studying other interactions of our compounds with other key-points belonging to the cell cytoskeleton. In particular, we investigated the possible implication of our complexes in regulating the actin dynamics in a direct way, and not as a consequence of the already observed interference with the tubulin polymerization reaction. Indeed, some microtubule poisons may promote the reorganization of the actin system, which is a consequent effect rather than a direct interaction. In other words, the microtubule metabolism can influence the organization, spatial distribution, and function of the nearby actin filaments [46]. With this in mind, we started with *in silico* studies that allowed us to assume that both complexes may bind the actin, sharing the same binding site of LA, used as the reference molecule. In particular, **AuL4** is positioned inside the nucleotide-binding site of actin, whereas **AuL7** exposes part of its structure to the solvent.

Next, we performed immunofluorescence assays in the two cancer cell models above-mentioned. The outcomes suggest that both complexes induced dramatic changes in actin organization; indeed, the filaments appeared thicker and with an abnormal spatial distribution, with respect to the control-treated cells, and in a similar rearrangement produced by LA treatment. In order to fully understand if these changes were due to a direct effect rather than the already studied interference with the tubulin polymerization reaction, we carried out some direct enzymatic assays on the purified rabbit actin, so that any other possible secondary effect could be excluded. Effectively, both complexes inhibited the actin polymerization in a similar extent to the CB, but lesser than LA, used as reference molecules. Conversely to LA, **AuL4** and **AuL7** were not able to promote the F-actin depolymerization. In conclusion, both the complexes inhibited the actin polymerization directly, but not the inverse reaction, and induced dramatic change in the organization and function of the actin system; this is a feature that discloses another—and not foreseen—important anticancer target of our NHC-gold complexes.

5. Conclusions

Herein, we reported evidence that the NHC-gold complexes **AuL4** and **AuL7** are inhibitors of the actin polymerization reaction with similar efficacy of CB, but do not accelerate the rate of F-actin depolymerization, as it happens for the LA. These complexes induce dramatic changes in cell morphology, triggering the formation of abnormal actin structures. We strongly believe that this evidence contributes to better knowledge of the variety of intracellular targets in the cancer fight.

Author Contributions: Conceptualization, M.S.S.; methodology, D.I.; software, C.R. and M.S.; validation, P.L., formal analysis, J.C. and A.M.; investigation, J.C.; data curation, A.C. and M.S.S.; writing—original draft preparation, D.I. and J.C.; writing—review and editing, S.A.; visualization, C.S. and M.P.; supervision, M.S.S.; project administration, P.L.; funding acquisition, C.R. All authors have read and agreed to the published version of the manuscript.

Funding: C.R. acknowledges the support by a grant from the Italian Ministry of Health (Ricerca Corrente 2020).

Institutional Review Board Statement: Not Applicable.

Informed Consent Statement: Not Applicable.

Data Availability Statement: Not Applicable.

Conflicts of Interest: The authors declare no conflict of interest.

References

1. Jakupec, M.A.; Galanski, M.; Arion, V.B.; Hartinger, C.G.; Keppler, B.K. Antitumour metal compounds: More than theme and variations. *Dalton Trans.* **2008**, 183–194. [\[CrossRef\]](#)
2. Wang, D.; Lippard, S.J. Cellular processing of platinum anticancer drugs. *Nat. Rev. Drug Discov.* **2005**, *4*, 307–320. [\[CrossRef\]](#) [\[PubMed\]](#)
3. Zeglis, B.M.; Pierre, V.C.; Barton, J.K. Metallo-intercalators and metallo-insertors. *Chem. Commun.* **2007**, *44*, 4565–4579. [\[CrossRef\]](#) [\[PubMed\]](#)
4. Bertrand, B.; Casini, A. A golden future in medicinal inorganic chemistry: The promise of anticancer gold organometallic compounds. *Dalton Trans.* **2014**, *43*, 4209–4219. [\[CrossRef\]](#) [\[PubMed\]](#)
5. Gaynor, D.; Griffith, D.M. The prevalence of metal-based drugs as therapeutic or diagnostic agents: Beyond platinum. *Dalton Trans.* **2012**, *41*, 13239–13257. [\[CrossRef\]](#)
6. Orvig, C.; Abrams, M.J. Medicinal inorganic chemistry: Introduction. *Chem. Rev.* **1999**, *99*, 2201–2204. [\[CrossRef\]](#) [\[PubMed\]](#)
7. Gottlieb, N.L. Comparative pharmacokinetics of parenteral and oral gold compounds. *J. Rheumatol. Suppl.* **1982**, *8*, 99–109.
8. Hindi, K.M.; Panzner, M.J.; Tessier, C.A.; Cannon, C.L.; Youngs, W.J. The medicinal applications of imidazolium carbene-metal complexes. *Chem. Rev.* **2009**, *109*, 3859–3884. [\[CrossRef\]](#)
9. Liu, W.; Gust, R. Metal N-heterocyclic carbene complexes as potential antitumor metallodrugs. *Chem. Soc. Rev.* **2013**, *42*, 755–773. [\[CrossRef\]](#)
10. Ceramella, J.; Mariconda, A.; Iacopetta, D.; Saturnino, C.; Barbarossa, A.; Caruso, A.; Rosano, C.; Sinicropi, M.S.; Longo, P. From coins to cancer therapy: Gold, silver and copper complexes targeting human topoisomerases. *Bioorg. Med. Chem. Lett.* **2020**, *30*, 126905. [\[CrossRef\]](#)
11. Hickey, J.L.; Ruhayel, R.A.; Barnard, P.J.; Baker, M.V.; Berners-Price, S.J.; Filipovska, A. Mitochondria-targeted chemotherapeutics: The rational design of gold(I) N-heterocyclic carbene complexes that are selectively toxic to cancer cells and target protein selenols in preference to thiols. *J. Am. Chem. Soc.* **2008**, *130*, 12570–12571. [\[CrossRef\]](#) [\[PubMed\]](#)
12. Barnard, P.J.; Berners-Price, S.J. Targeting the mitochondrial cell death pathway with gold compounds. *Coord. Chem. Rev.* **2007**, *251*, 1889–1902. [\[CrossRef\]](#)
13. Krishnamurthy, D.; Karver, M.R.; Fiorillo, E.; Orru, V.; Stanford, S.M.; Bottini, N.; Barrios, A.M. Gold(I)-mediated inhibition of protein tyrosine phosphatases: A detailed in vitro and cellular study. *J. Med. Chem.* **2008**, *51*, 4790–4795. [\[CrossRef\]](#) [\[PubMed\]](#)
14. Fung, S.K.; Zou, T.; Cao, B.; Lee, P.Y.; Fung, Y.M.; Hu, D.; Lok, C.N.; Che, C.M. Cyclometalated Gold(III) Complexes Containing N-Heterocyclic Carbene Ligands Engage Multiple Anti-Cancer Molecular Targets. *Angew. Chem. Int. Ed. Engl.* **2017**, *56*, 3892–3896. [\[CrossRef\]](#) [\[PubMed\]](#)
15. Iacopetta, D.; Rosano, C.; Sirignano, M.; Mariconda, A.; Ceramella, J.; Ponassi, M.; Saturnino, C.; Sinicropi, M.S.; Longo, P. Is the Way to Fight Cancer Paved with Gold? Metal-Based Carbene Complexes with Multiple and Fascinating Biological Features. *Pharmaceuticals* **2020**, *13*, 91. [\[CrossRef\]](#)
16. Magherini, F.; Fiaschi, T.; Valocchia, E.; Becatti, M.; Pratesi, A.; Marzo, T.; Massai, L.; Gabbiani, C.; Landini, I.; Nobili, S.; et al. Antiproliferative effects of two gold(I)-N-heterocyclic carbene complexes in A2780 human ovarian cancer cells: A comparative proteomic study. *Oncotarget* **2018**, *9*, 28042–28068. [\[CrossRef\]](#)
17. Muenzner, J.K.; Biersack, B.; Albrecht, A.; Rehm, T.; Lacher, U.; Milius, W.; Casini, A.; Zhang, J.J.; Ott, I.; Brabec, V.; et al. Ferrocenyl-Coupled N-Heterocyclic Carbene Complexes of Gold(I): A Successful Approach to Multinuclear Anticancer Drugs. *Chemistry* **2016**, *22*, 18953–18962. [\[CrossRef\]](#)
18. Iacopetta, D.; Mariconda, A.; Saturnino, C.; Caruso, A.; Palma, G.; Ceramella, J.; Muia, N.; Perri, M.; Sinicropi, M.S.; Caroleo, M.C.; et al. Novel Gold and Silver Carbene Complexes Exert Antitumor Effects Triggering the Reactive Oxygen Species Dependent Intrinsic Apoptotic Pathway. *ChemMedChem* **2017**, *12*, 2054–2065. [\[CrossRef\]](#)
19. Dhamodharan, R.; Jordan, M.A.; Thrower, D.; Wilson, L.; Wadsworth, P. Vinblastine suppresses dynamics of individual microtubules in living interphase cells. *Mol. Biol. Cell* **1995**, *6*, 1215–1229. [\[CrossRef\]](#)
20. Rizza, P.; Pellegrino, M.; Caruso, A.; Iacopetta, D.; Sinicropi, M.S.; Rault, S.; Lancelot, J.C.; El-Kashef, H.; Lesnard, A.; Rochais, C.; et al. 3-(Dipropylamino)-5-hydroxybenzofuro[2,3-f]quinazolin-1(2H)-one (DPA-HBFQ-1) plays an inhibitory role on breast cancer cell growth and progression. *Eur. J. Med. Chem.* **2016**, *107*, 275–287. [\[CrossRef\]](#)
21. Ceramella, J.; Caruso, A.; Occhiuzzi, M.A.; Iacopetta, D.; Barbarossa, A.; Rizzuti, B.; Dallemagne, P.; Rault, S.; El-Kashef, H.; Saturnino, C.; et al. Benzothienoquinazolinones as new multi-target scaffolds: Dual inhibition of human Topoisomerase I and tubulin polymerization. *Eur. J. Med. Chem.* **2019**, *181*, 111583. [\[CrossRef\]](#) [\[PubMed\]](#)
22. Rebowski, G.; Boczkowska, M.; Drazic, A.; Ree, R.; Goris, M.; Arnesen, T.; Dominguez, R. Mechanism of actin N-terminal acetylation. *Sci. Adv.* **2020**, *6*, eaay8793. [\[CrossRef\]](#)

23. Morris, G.M.; Huey, R.; Lindstrom, W.; Sanner, M.F.; Belew, R.K.; Goodsell, D.S.; Olson, A.J. AutoDock4 and AutoDockTools4: Automated docking with selective receptor flexibility. *J. Comput. Chem.* **2009**, *30*, 2785–2791. [[CrossRef](#)] [[PubMed](#)]
24. Sanner, M.F.; Duncan, B.S.; Carrillo, C.J.; Olson, A.J. Integrating computation and visualization for biomolecular analysis: An example using python and AVS. *Pac. Symp. Biocomput.* **1999**, 401–412. [[CrossRef](#)]
25. Cesarini, S.; Spallarossa, A.; Ranise, A.; Schenone, S.; Rosano, C.; La Colla, P.; Sanna, G.; Busonera, B.; Loddo, R. N-acylated and N,N'-diacylated imidazolidine-2-thione derivatives and N,N'-diacylated tetrahydropyrimidine-2(1H)-thione analogues: Synthesis and antiproliferative activity. *Eur. J. Med. Chem.* **2009**, *44*, 1106–1118. [[CrossRef](#)]
26. Rosano, C.; Hunt, M.J.O.; Brach, J.; Newman, A.B.; Studenski, S.; Verghese, J.; Weissfeld, L. Brain Anatomical Correlates of Gait Variability in High Functioning Older Adults: Repeatability across Two Independent Studies (Cns). *Gerontologist* **2012**, *52*, 319–320.
27. Pettersen, E.F.; Goddard, T.D.; Huang, C.C.; Couch, G.S.; Greenblatt, D.M.; Meng, E.C.; Ferrin, T.E. UCSF Chimera—A visualization system for exploratory research and analysis. *J. Comput. Chem.* **2004**, *25*, 1605–1612. [[CrossRef](#)]
28. Ceramella, J.; Loizzo, M.R.; Iacopetta, D.; Bonesi, M.; Sicari, V.; Pellicano, T.M.; Saturnino, C.; Malzert-Freon, A.; Tundis, R.; Sinicropi, M.S. *Anchusa azurea* Mill. (Boraginaceae) aerial parts methanol extract interfering with cytoskeleton organization induces programmed cancer cells death. *Food Funct.* **2019**, *10*, 4280–4290. [[CrossRef](#)] [[PubMed](#)]
29. Lappano, R.; Rosano, C.; Pisano, A.; Santolla, M.F.; De Francesco, E.M.; De Marco, P.; Dolce, V.; Ponassi, M.; Felli, L.; Cafeo, G.; et al. A calixpyrrole derivative acts as an antagonist to GPER, a G-protein coupled receptor: Mechanisms and models. *Dis. Model Mech.* **2015**, *8*, 1237–1246. [[CrossRef](#)] [[PubMed](#)]
30. Sinicropi, M.S.; Lappano, R.; Caruso, A.; Santolla, M.F.; Pisano, A.; Rosano, C.; Capasso, A.; Panno, A.; Lancelot, J.C.; Rault, S.; et al. (6-bromo-1,4-dimethyl-9H-carbazol-3-yl-methylene)-hydrazine (carbhydraz) acts as a GPER agonist in breast cancer cells. *Curr. Top. Med. Chem.* **2015**, *15*, 1035–1042. [[CrossRef](#)]
31. Stec-Martyna, E.; Ponassi, M.; Miele, M.; Parodi, S.; Felli, L.; Rosano, C. Structural comparison of the interaction of tubulin with various ligands affecting microtubule dynamics. *Curr. Cancer Drug Targets* **2012**, *12*, 658–666. [[CrossRef](#)] [[PubMed](#)]
32. Acharya, S.; Maji, M.; Raturaj, Purkait, K.; Gupta, A.; Mukherjee, A. Synthesis, Structure, Stability, and Inhibition of Tubulin Polymerization by Ru(II)-p-Cymene Complexes of Trimethoxyaniline-Based Schiff Bases. *Inorg. Chem.* **2019**, *58*, 9213–9224. [[CrossRef](#)] [[PubMed](#)]
33. Ceresa, C.; Nicolini, G.; Semperboni, S.; Gandin, V.; Monfrini, M.; Avezza, F.; Alberti, P.; Bravin, A.; Pellei, M.; Santini, C.; et al. Evaluation of the Profile and Mechanism of Neurotoxicity of Water-Soluble [Cu(P4)PF6 and [Au(P4)PF6 (P = thp or PTA) Anticancer Complexes. *Neurotox Res.* **2018**, *34*, 93–108. [[CrossRef](#)] [[PubMed](#)]
34. Kaps, L.; Biersack, B.; Muller-Bunz, H.; Mahal, K.; Munzner, J.; Tacke, M.; Mueller, T.; Schobert, R. Gold(I)-NHC complexes of antitumoral diarylimidazoles: Structures, cellular uptake routes and anticancer activities. *J. Inorg. Biochem.* **2012**, *106*, 52–58. [[CrossRef](#)]
35. Khanna, S.; Jana, B.; Saha, A.; Kurkute, P.; Ghosh, S.; Verma, S. Targeting cytotoxicity and tubulin polymerization by metal-carbene complexes on a purine tautomer platform. *Dalton Trans.* **2014**, *43*, 9838–9842. [[CrossRef](#)]
36. Muenzner, J.K.; Biersack, B.; Kalie, H.; Andronache, I.C.; Kaps, L.; Schuppan, D.; Sasse, F.; Schobert, R. Gold(I) biscarbene complexes derived from vascular-disrupting combretastatin A-4 address different targets and show antimetastatic potential. *ChemMedChem* **2014**, *9*, 1195–1204. [[CrossRef](#)] [[PubMed](#)]
37. Cheng, X.; Haerberle, S.; Shytaj, I.L.; Gama-Brambila, R.A.; Theobald, J.; Ghafoory, S.; Wolker, J.; Basu, U.; Schmidt, C.; Timm, A.; et al. NHC-gold compounds mediate immune suppression through induction of AHR-TGFbeta1 signalling in vitro and in scurfy mice. *Commun. Biol.* **2020**, *3*, 10. [[CrossRef](#)]
38. Pasquier, E.; Kavallaris, M. Microtubules: A dynamic target in cancer therapy. *IUBMB Life* **2008**, *60*, 165–170. [[CrossRef](#)] [[PubMed](#)]
39. Fenteany, G.; Zhu, S. Small-molecule inhibitors of actin dynamics and cell motility. *Curr. Top. Med. Chem.* **2003**, *3*, 593–616. [[CrossRef](#)]
40. Aseervatham, J. Cytoskeletal Remodeling in Cancer. *Biology* **2020**, *9*, 385. [[CrossRef](#)]
41. Yamaguchi, H.; Condeelis, J. Regulation of the actin cytoskeleton in cancer cell migration and invasion. *Biochim. Biophys. Acta* **2007**, *1773*, 642–652. [[CrossRef](#)] [[PubMed](#)]
42. Olson, M.F.; Sahai, E. The actin cytoskeleton in cancer cell motility. *Clin. Exp. Metastasis* **2009**, *26*, 273–287. [[CrossRef](#)] [[PubMed](#)]
43. Rosenblum, M.D.; Shivers, R.R. 'Rings' of F-actin form around the nucleus in cultured human MCF7 adenocarcinoma cells upon exposure to both taxol and taxotere. *Comp. Biochem. Physiol. Part C Pharmacol. Toxicol. Endocrinol.* **2000**, *125*, 121–131. [[CrossRef](#)]
44. Foissner, I.; Wasteneys, G.O. Wide-ranging effects of eight cytochalasins and latrunculin A and B on intracellular motility and actin filament reorganization in characean internodal cells. *Plant Cell Physiol.* **2007**, *48*, 585–597. [[CrossRef](#)]
45. Fujiwara, I.; Zweifel, M.E.; Courtemanche, N.; Pollard, T.D. Latrunculin A Accelerates Actin Filament Depolymerization in Addition to Sequestering Actin Monomers. *Curr. Biol.* **2018**, *28*, 3183–3192. [[CrossRef](#)]
46. Danowski, B.A. Fibroblast contractility and actin organization are stimulated by microtubule inhibitors. *J. Cell Sci.* **1989**, *93 Pt 2*, 255–266. [[CrossRef](#)]